


Star polymers as unit cells for coarse-graining cross-linked networks

Taras Y. Molotilin,¹ Salim R. Maduar,¹ and Olga I. Vinogradova^{1,2,3,*}

¹*A.N. Frumkin Institute of Physical Chemistry and Electrochemistry, Russian Academy of Sciences, 31 Leninsky Prospekt, 119071 Moscow, Russia*

²*Department of Physics, M.V. Lomonosov Moscow State University, 119991 Moscow, Russia*

³*DWI–Leibniz Institute for Interactive Materials, Forckenbeckstrasse 50, 52056 Aachen, Germany*

 (Received 7 September 2016; revised manuscript received 20 February 2018; published 13 March 2018)

Reducing the complexity of cross-linked polymer networks by preserving their main macroscale properties is key to understanding them, and a crucial issue is to relate individual properties of the polymer constituents to those of the reduced network. Here we study polymer networks in a good solvent, by considering star polymers as their unit elements, and first quantify the interaction between their centers of masses. We then reduce the complexity of a network by replacing sets of its bridged star polymers by equivalent effective soft particles with dense cores. Our coarse graining allows us to approximate complex polymer networks by much simpler ones, keeping their relevant mechanical properties, as illustrated in computer experiments.

DOI: [10.1103/PhysRevE.97.032504](https://doi.org/10.1103/PhysRevE.97.032504)

I. INTRODUCTION

One of the most difficult hurdles in the computer investigation of cross-linked polymer networks, i.e., gels, is, understandably, the prohibitively long simulation time due to a large amount of particles (monomers) in the system. Explicit simulations are currently limited by nanogels with low degree of polymerization ($N \leq 15$) [1,2]. Larger systems, even microgels, represent a challenge or become impossible to deal with. A promising way to attack this problem is to coarse-grain the complex network by mapping it into a simpler one, i.e., to reduce the number of particles while preserving macroscale properties. However, general principles of such a coarse-graining have not yet been established. Some of the existing methods are currently capable to simulate only a part of a network in a periodic box [3–6]. Others do not relate the collective response of large-scale networks to individual properties of their polymer constituents [7].

The cross-linked network represents an aggregate of low-branched star polymers (SPs) connected by bridges, so that the pair interaction of network SPs could potentially be used to construct a coarse-graining scheme. The interaction between SPs has been studied by several groups. Most of this work focused on highly branched stars with large “dense” central core. It has been found that at short separations the potential of mean force shows a logarithmic decay and scales with functionality as $f^{3/2}$ [8]. Later, a potential of mean force between two SPs that combines a short range logarithmic repulsion with a soft Yukawa-type tail has been proposed and extensively tested [9]. The body of work investigating low-branched SPs remains rather scarce. A few authors made important remarks that properties of low-branched SPs could differ from those of highly branched [10–12]. Thus, when $f \leq 10$ the monomer density around the central bead is no longer described by the

blob model, and the Yukawa-type repulsion is not observed [10,13]. We should note that contrary to interacting linear chains, where coordinates associated with the centers of mass are normally employed [14–17], previous studies of SPs have commonly used coordinates related to central beads [9,10]. Although some investigations of low-branched stars [13,18] have used the center of mass approach, they did not attempt to predict star interaction energies. Finally, we note that prior work concerned an interaction of SPs in solutions only and not attempted to calculate it for SPs, constituting the network.

In this paper we propose a procedure to coarse-grain polymer networks in a good solvent, based on the idea of mapping their low-branched SPs to effective particles. Our concept is based on the analysis of interactions between two network SPs, by using their centers of mass as effective coordinates (see Fig. 1). We obtain expressions for potentials of mean force, which define a coarse-grained model, and validate them by explicit (monomer-resolved) simulations. Finally, we study a mechanical deformation of the reduced polymer networks and show that the coarse-graining provides a highly representative approximation of the initial network, by dramatically reducing an amount of particles in simulations.

Our paper is organized as follows: Section II describes and validates our theory for ideal networks composed of identical SPs, which have received much attention in recent years [19,20]. The power of our approach is illustrated in Sec. III, where we study an isotropic extension and compression of ideal networks. In Sec. IV we discuss the extension of our coarse-grained model to random networks composed of SPs of different functionalities, and consider their uniaxial extension and compression. We conclude in Sec. V with a discussion of our results and their possible extensions to more complex systems. Appendix A contains the derivation of the equation that determines root mean-squared deviation of the central bead from the SP’s center of mass. The details of explicit Monte Carlo (MC) simulations employed to measure the potential of mean force are given in Appendix B. In Appendix C we derive

*Corresponding author: oivinograd@yahoo.com

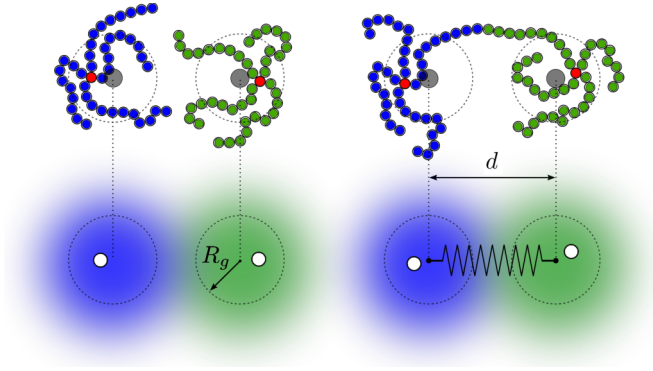


FIG. 1. Sketch of interacting star polymers of R_g separated by distance d . Explicit bead-spring models are shown at the top, and coarse-grained models—at the bottom. Gray and white circles indicate central beads, centers of mass, and “dense” cores.

the equation, that determines the probability of collision of SP’s dense cores. Appendix D describes explicit and coarse-grained molecular dynamics (MD) simulations of cross-linked networks.

II. INTERACTIONS OF IDENTICAL STAR POLYMERS

To show the basic principles of the approach in compact terms we consider two interacting identical SPs of fixed (to arbitrary values) f and N in a good solvent. Although the SPs are normally defined for $f \geq 3$, we also consider a special case of $f = 2$, which corresponds to a linear polymer chain of a degree of polymerisation $2N$.

A. The choice of effective coordinates

We first justify the choice of our effective coordinates. Note that the time average location of the center of mass of an SP does of course coincide with that of the central bead, but its instantaneous position deviates from the central bead location (see Appendix A). This can be illustrated by explicit (with monomers of size σ) MC simulations of single SPs with different f and N (see Appendix B for details). The simulation data plotted in Fig. 2 shows discernible deviations of a central bead from the center of mass, which, however, tend to decrease with f . A corollary from this is that the mean-squared distance Δ^2 between the center of mass and the core is finite. Indeed,

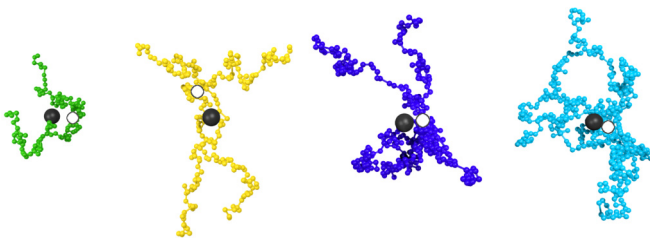


FIG. 2. Simulation snapshots of star polymers with $N = 33$ and $f = 2, 4, 6, 8$. Large beads indicate the centers of mass. White beads are the central cores.

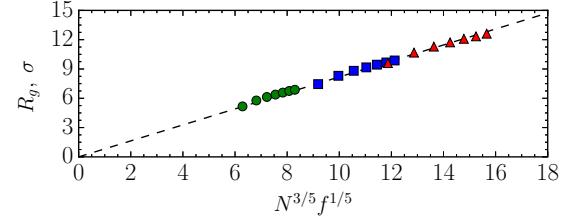


FIG. 3. Radii of gyration obtained in MC simulations for star polymers of $N = 17$ (circles), 32 (squares), and 49 (triangles). Symbols from left to right show data for f from 2 to 8 . Dashed line corresponds to the scaling relationship $R_g \propto N^{3/5} f^{1/5}$.

one can show using mean-field arguments that Δ scales with f as

$$\Delta = A f^{-7/10} R_g, \quad (1)$$

which indicates that Δ could be comparable with the radii of gyration, R_g . To prove this we have first measured R_g in simulations and plotted it in Fig. 3. One can see that our data agrees well with the scaling law, $R_g \propto N^\nu f^{1/5}$ (with the Flory exponent $\nu \simeq 3/5$), suggested earlier for SPs in a good solvent [21]. We have then obtained the values of Δ (see Fig. 4) and fitted the simulation data to Eq. (1), taking A as a fitting parameter. The theoretical curve is included in Fig. 4 and the value $A = 1.07$ has been obtained from fitting. This is close to $A = 2^{-2/5} \sqrt{11/5} \simeq 1.12$ predicted by our mean-field theory (see Appendix A). These results demonstrate that the central bead fluctuates around the center of mass, which is especially pronounced at low f , so that below we use the centers of mass as effective coordinates.

B. Interaction of star polymers in solutions

Let us now investigate the effect of functionality on the value of the interaction free energy F_1 of two SPs as a function of separation d between their centers of mass. This has been calculated by using the histogram method with a bias potential to ensure efficient sampling of configuration space [22,23] as described in Appendix B. In Fig. 5 we plot simulation results obtained at fixed $N = 17$ and f varying from 2 to 8 . The data show that the two SPs always repel each other, and that the value of F_1 increases with f . Remarkably, it remains finite at zero separation, i.e., when centers of mass overlap, and there is no manifestation of logarithmic divergence at $d = 0$ predicted

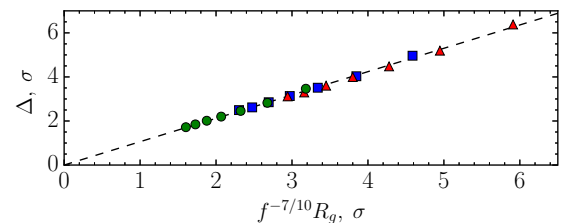


FIG. 4. Root mean-squared distance between the center of mass and the central bead of a star polymer of functionality $f = 2-8$ obtained in MC simulations. Circles show simulation data for $N = 17$; squares for $N = 32$; and triangles for $N = 49$. Dashed line plots predictions of Eq. (1).

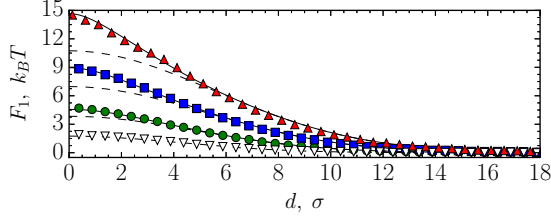


FIG. 5. Interaction potentials F_1 between star polymers of $N = 17$ obtained in simulations (symbols). From top to bottom $f = 8, 6, 4, 2$. Dashed curves show F^{ss} predicted by Eq. (3), solid curves are fits to Eq. (6).

when central beads are chosen as effective coordinates [24]. We note that the repulsion of SPs in our case resembles that of linear chains [16].

To interpret the simulation data we first consider the long-range or “soft-sphere” part of interaction, which is attributed to SP’s coronas. In the case of linear chains, $f = 2$, the interaction free energy can be represented by a Gaussian function, $F_1 = F^{\text{ss}} = F_0 \exp(-3d^2/4R_g^2)$ [25], with a range of the order of R_g [15,16] and $F_0 \simeq 1.53k_B T$ found theoretically [17]. Note, however, that some simulations have deduced $F_0 \simeq 1.9k_B T$ [14,16]. The scaling expression for F_0 in the case of SPs can be estimated using average number of contacts between monomers, corrected for their correlations, as [26,27]

$$\frac{F_0}{k_B T} \propto \rho V (\rho a^3)^{1/(3\nu-1)} \simeq \frac{f^{9/4} N^{9/4}}{R_g^{15/4}}, \quad (2)$$

where we have used $V \simeq R_g^3$ for the overlap volume and $\rho \propto fN/R_g^3$ for monomer density. By substituting scaling expressions for R_g into Eq. (2) we obtain $F_0 \propto f^{3/2}$ and the “soft-sphere” interaction free energy becomes similar to known for interacting linear polymers:

$$F^{\text{ss}} = F_0 \exp\left(-\frac{3d^2}{4R_g^2}\right), \quad (3)$$

but includes F_0 , which depends on f . Note, however, that F_0 does not depend on N , which is similar to results for linear polymers [16,27].

Calculations made using Eq. (3) with F_0 taken as adjustable parameters for the long-range tails are included in Fig. 5. We see that simulation data at large d are indeed well described by a Gaussian repulsion with R_g found above (see Fig. 3). To verify the scaling relationship for $F_0 = F^{\text{ss}}(0)$ we now plot it in Fig. 6 as a function of $f^{3/2}$. Also included are additional simulation data for $N = 25$ and 49. These data allows us to deduce the universal value of $F_0 = (0.48 \pm 0.03) f^{3/2} k_B T$, which is valid for all f and does not depend on N . Figure 6 also includes the SPs interaction free energy, F_1 , obtained from simulation data at $d = 0$. One can conclude that for all N deviations of $F(0)$ from F_0 are negligibly small when $f = 2$ and 3, but they become discernible at larger functionalities, and their values increase with f . The discrepancy is always in the direction of larger potential than F_0 .

We remark that deviations of F_1 from F^{ss} given by Eq. (3) are observed only at small d as seen yet in Fig. 5. An explanation can be obtained if we invoke the short-range

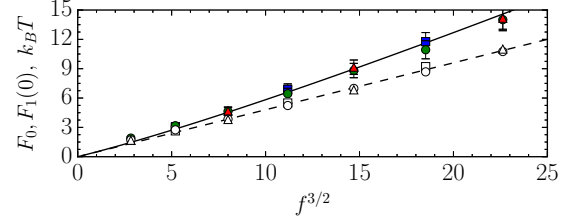


FIG. 6. Amplitude of the “soft-sphere” (open symbols) and total (closed symbols) potential as a function of $f^{3/2}$ for $N = 17$ (circles), 25 (squares), and 49 (triangles). Solid and dashed lines are added to guide the eye.

repulsion emerging when SPs strongly overlap, so that the effective interaction between their “dense” cores becomes important. For simplicity we model the entropic short-range logarithmic interaction of the cores [8] by describing them as “hard spheres” of an effective radius σ_c .

Then each “dense” core may be seen as a Brownian particle of diffusion coefficient D fluctuating around the center of mass with zero mean, but finite variance, Δ^2 , see Eq. (4). The interaction free energy is then given by $F^{\text{hs}} = -k_B T \ln(1 - P)$, where $P(t, d)$ is the probability for a collision of two dense cores, initially separated by distance d , to occur after time t given by $6Dt = \Delta^2$. Thereby, in F^{hs} we exclude configurations where cores approach closer than $2\sigma_c$. The solution for P may be found by considering properties of diffusing particles (see Appendix C for details of derivation):

$$P = \frac{1}{2} \text{erf}(y_-) - \frac{1}{2} \text{erf}(y_+) + \sqrt{\frac{\Delta^2}{3\pi d^2}} (e^{-y_+^2} - e^{-y_-^2}), \quad (4)$$

where $y_{\pm} = \sqrt{3} \frac{d \pm 2\sigma_c}{2\Delta}$. For small f or for $\sigma_c/\Delta \ll 1$ the interaction free energy of “dense” cores reduces to a Gaussian function:

$$F^{\text{hs}} = k_B T \frac{4\sqrt{3}}{\sqrt{\pi}} \exp\left(-\frac{3d^2}{4\Delta^2}\right) \left(\frac{\sigma_c}{\Delta}\right)^3. \quad (5)$$

We remark that although the cores are represented by “hard spheres,” their interaction free energy may still be finite at $d = 0$. In our simulations we found that $\sigma_c/\Delta \simeq Bf$, so it is independent on N . Here B is constant for all f, N which was found to be equal to $\simeq 0.16 \pm 0.02$. This implies that σ_c scales as $f^{1/2}$, which is in agreement with prior work [21]. We also note that with our parameters for $f = 2$ we have $\sigma_c/\Delta \simeq 0.3$, so that at $d = 0$ this gives $F^{\text{hs}} \simeq 0.1k_B T$, which is much smaller than F_0 and can safely be neglected. Equation (5) can be used to describe SPs up to $f = 4$. Finally, in the limit of large f our Eq. (4) reduces to the “hard-sphere” interaction potential. We should like to stress that unlike logarithmic repulsion, F^{hs} vanishes at large d , so that we do not need to adjust the cut-off distance for a short-range interaction as it has been done before [9].

Now combining both soft-sphere and hard-sphere repulsions we can propose the repulsive potential of mean force for two SPs

$$F_1 = F^{\text{ss}} + F^{\text{hs}} \quad (6)$$

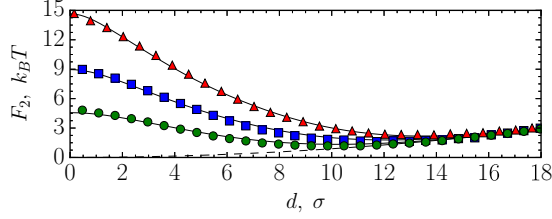


FIG. 7. Interaction potential of two SPs connected by a bridge of $2N = 34$ (symbols). From top to bottom $f = 8, 6$, and 4 . Solid curve shows calculations with Eq. (7). Dashed curves plots bridging attraction given by Eq. (8).

with F^{ss} and F^{hs} defined by Eqs.(3) and (5). Theoretical curves calculated with Eq. (6) are included in Fig. 5. We see that our model is in excellent agreement with simulation data for all d .

C. Interaction of star polymers in networks

We finally turn to two SPs as a network segment. The important difference from the solutions is the bridging of SPs, which should give rise to an additional attraction between them. This bridging attraction, F^b , should be added to Eq. (6) to give

$$F_2 = F^{\text{ss}} + F^{\text{hs}} + F^b. \quad (7)$$

As long as $d \ll 2N\sigma$, F^b can be estimated as the free energy of stretching of a linear chain

$$F^b = \frac{kd^2}{2}, \quad (8)$$

where $k = 3k_B T/R_F^2$ with $R_F \simeq (2N)^\nu \sigma$ [28,29], but note that for very large $d \gg R_g$ one has to define F^b differently [30,31]. We also stress that since the bridging attraction is long-range, $d \gg \Delta$. Therefore, this contribution does not depend on the choice of coordinates.

To verify the model we have simulated the potentials of mean force between two SPs of f varying from 2 to 8 connected via a bridge of fixed $2N = 34$. The values of F obtained in simulations are plotted in Fig. 7. This plot also includes theoretical curves calculated with Eq. (7). The calculations are made using R_g shown in Fig. 3 and the ratio $R_g^2/R_F^2 \simeq 0.157$ [32] leading to $k \simeq 1.22N^{-6/5}k_B T/\sigma^2$. In other words, there are no adjustable parameters in the theoretical curves. We see that the fits are very good for all d , which confirms the validity of our model. Another important conclusion from Fig. 7 is that F_2 has a minimum at $d_0 \simeq 2R_g \sqrt{\ln(3F_0/2kR_g^2)}/\sqrt{3}$, which corresponds to the equilibrium position of two SPs. Therefore, they may be seen as an effective spring of a constant $k_{\text{eff}} \simeq 2k \ln(3F_0/2kR_g^2)$. To verify the model for k we have made simulations for SPs of $f = 2$ and 4 , and N varying from 17 to 49, and found that results fully confirm our theory (see Fig. 8).

III. COARSE-GRAINING OF IDEAL POLYMER NETWORKS

Altogether the above results suggest that a polymer network segments (SPs) can be effectively represented by soft Gaussian spheres with “hard” cores connected by springs. To prove that interaction potentials of two SPs indeed define an efficient

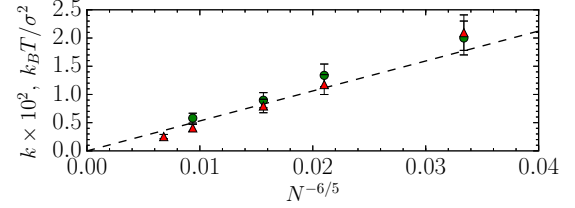


FIG. 8. Effective stiffness of a bridge as a function of N (varied from 17 to 49) obtained in simulations. Circles show results for $f = 4$; triangles for $f = 2$. Dashed line plots predictions of Eq. (8) in the main text.

coarse-grained model, below we compare elastic properties of an explicit SP network with that of an ideal coarse-grained network. MD simulations of a deformed ideal cross-linked network is performed using an open-source package ESPResSo [33]. Below we will only present our main results, and the details of explicit and coarse-grained simulation models can be found in Appendix D.

Specifically, we study an isotropic deformation of a cubic network constituted of SPs with $f = 6$ connected by bridges of $2N = 34$ as shown in Fig. 9(a). We measure an excess pressure, Π , due to compression and extension as a function of the size of the unit cell L . We also perform the coarse-grained simulations, where we replace the network SPs by effective spheres interacting with each other with potential F_2 , which reduces the number of particles in fN times and therefore significantly accelerates calculations. The detailed comparison between the explicit simulation results and the coarse-graining approach is then shown in Fig. 10. A general conclusion from this plot is that the coarse-graining data are in excellent agreement with explicit simulation results. Note that one can also roughly evaluate pressure theoretically as

$$\Pi = -\frac{f}{2}dF_2/dV, \quad (9)$$

i.e., by neglecting interactions of SPs, which are not connected by bridges. Here $f/2$ is the number of bridges in volume $V = L^3$. These estimates are also included in Fig. 10, and show that this simple theory agrees well with simulation data for $L/d_0 = O(1)$ and larger, i.e., for stretching. However, F_1 cannot be ignored in the case of compression, i.e., small L/d_0 .

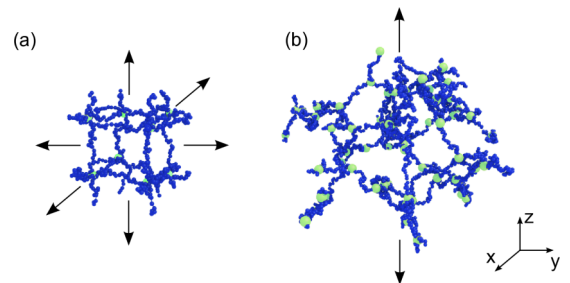


FIG. 9. Simulation snapshots of an ideal cubic polymer network with $f = 6$ (a) and of a random network with f varying from 3 to 7 (b). In both cases $2N = 34$. Arrows indicate the direction of deformation: An ideal network is subjected to an isotropic strain and a random network is deformed along the z axis.

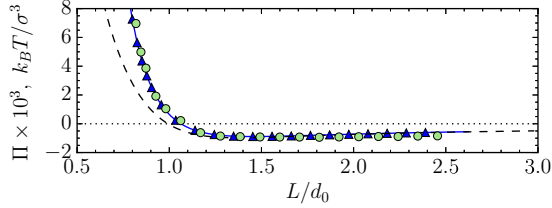


FIG. 10. Excess pressure of the ideal cubic network ($N = 17$, $f = 6$, $d_0 \simeq 12.1\sigma$) under an isotropic deformation as a function of L/d_0 . Triangles plot the results of the coarse-grained model, solid curve is a polynomial fit shown as a guide for the eye. Circles show the results of explicit simulations. Dashed curve shows predictions of Eq. (9).

IV. TOWARD THE DESCRIPTION AND COARSE-GRAINING OF POLYDISPERSE NETWORKS

In the preceding sections, we have proposed and validated an efficient procedure to coarse-grain polymer networks. However, its general principles have been formulated assuming an ideal network composed of identical SPs and by studying its isotropic deformations. Although further extensions of our model to various complex situations is beyond the scope of the present paper, we illustrate how such extensions could be made by discussing the case of a random network constituted of SPs of a fixed N , but various f . In other words, we assume that two, i th and j th, interacting network SPs have functionalities $f_i \neq f_j$. We will also assume that f_i and f_j are of the same order of magnitude, which is the case of typical polymer gels.

To account for different functionalities of two interacting SPs in such a random network, some expressions for components of the coarse-grained potential, F_2 , described by Eq. (7), have to be modified. We first recall that F^b depends on N only, so that it remains the same for our polydisperse network of fixed N . In contrast, F_1 of our polydisperse network should now become functions of f_i and f_j . Provided $f_i/f_j = O(1)$, one can generalize Eq. (2) to

$$\frac{F_0}{k_B T} \propto \frac{\rho_i V_i (\rho_j a^3)^{1/(3v-1)} + \rho_j V_j (\rho_i a^3)^{1/(3v-1)}}{2},$$

which immediately leads to

$$\frac{F_0}{k_B T} \propto \frac{f_i f_j^{1/2} + f_j f_i^{1/2}}{2} \simeq (f_i f_j)^{3/4}. \quad (10)$$

This value of F_0 should be used in Eq. (3), which defines F^{ss} . Besides, R_g^{-2} in Eq. (3) should be substituted by $(R_{g,i}^{-2} + R_{g,j}^{-2})/2$, which can be easily argued by considering a convolution of two Gaussian density profiles of different SPs. Finally, in Eq. (5), which describes F^{hs} , Δ^2 should be substituted by $(\Delta_i^2 + \Delta_j^2)/2$, and σ_c should be replaced by $(\sigma_{c,i} + \sigma_{c,j})/2$.

To assess the validity of the above coarse-grained model for a polydisperse network, we now perform simulations of an anisotropic uniaxial compression and extension [as illustrated in Fig. 9(b)]. We study networks constituted of SPs with functionalities, which can take any value in the interval from 3 to 7 (see Appendix D). We first bring the system to a stress-free state, and then stretch or compress the simulation box along the z axis, while compressing or stretching it along x and y

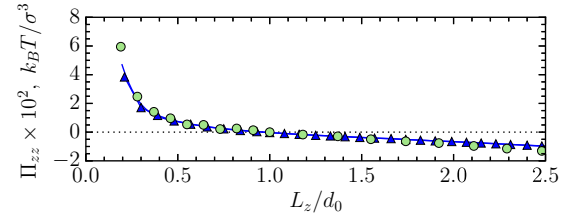


FIG. 11. Uniaxial extension and compression: zz component of the pressure tensor as a function of L_z/d_0 for a random network composed of SPs with $N = 17$ and f in the interval between 3 and 7. Triangles are results of the coarse-grained model. Solid curve is a polynomial fit added to guide the eye. Circles show results obtained in explicit simulations.

axes to conserve the volume of the system. Figure 11 shows the zz component of the pressure tensor Π_{zz} as a function of the relative deformation L_z/d_0 obtained by using explicit and coarse-grained simulations. Altogether the results of explicit and coarse-grained simulations agree very well, confirming the validity of our model.

V. CONCLUSION

In this paper we have calculated the free interaction energy of two identical SPs by using their centers of mass as effective coordinates. Our analysis has led to explicit expressions for interaction potentials of SPs of any f and N , and in the limiting case of $f = 2$ recovers known results for linear polymers. We have checked the validity of our theory by explicit MC simulations. These potentials have provided a framework for a coarse-graining approach, allowing one to reduce the number of particles in simulations in fN times. The advantages of our coarse-graining method have been illustrated by considering an isotropic compression and extension of an ideal polymer network.

Our approach can be extended to a more complex situation of a network with random topology. We have illustrated a strategy of such an extension by calculating the free interaction energy of two SPs of the same N , but different f , which defines a modified coarse-grained model, applicable for some random networks. We have demonstrated that the scaling expressions proposed for identical SPs constituting ideal networks may indeed be applied equally to SPs of different functionalities. In other words, interactions between SPs in random networks obey similar scaling laws, but, according to our analysis, some parameters in the interaction potentials should be substituted for their effective values. The extension of our model to a situation of a non-ideal polydisperse network composed of SPs of different N is currently under progress and will be published elsewhere.

Another fruitful direction could be to generalize our model to the case of weakly charged polyelectrolyte networks, and to employ it to study their mechanical properties. Finally, we mention that our approach can be immediately applied to study various properties of microgel particles.

ACKNOWLEDGMENTS

This work was partly supported by the Deutsche Forschungsgemeinschaft through SFB 985 ‘‘Functional mi-

crogels and microgel systems.” We thank O. V. Borisov and F. Schmid for helpful discussions and K. Binder for valuable comments on the manuscript. The simulations were carried out using computational resources at the Moscow State University (“Lomonosov” and “Chebyshev”).

APPENDIX A: DEVIATIONS OF THE CENTRAL BEAD FROM THE CENTER OF MASS

The mean-squared distance between the center of mass of a star and its central bead is defined as

$$\Delta^2 = \langle \mathbf{r}_c \cdot \mathbf{r}_c \rangle, \quad (\text{A1})$$

where \mathbf{r}_c is the instantaneous position of the center of mass relative to the central bead. This choice of the reference point implies that $\langle \mathbf{r}_c \rangle = 0$.

We can express \mathbf{r}_c using the positions of the SP’s arms’ centers of mass, $\mathbf{r}_{c,i}$,

$$\mathbf{r}_c = \frac{1}{fN} \sum_{j=1}^f \sum_{i=1}^N \mathbf{r}_{ij} = \sum_{j=1}^f \frac{\mathbf{r}_{c,j}}{f}. \quad (\text{A2})$$

Note that fN is the total number of monomers in a star. By substituting Eq. (A2) into Eq. (A1) and taking the statistical average we find

$$\Delta^2 \simeq \frac{1}{f^2} \sum_{j=0}^f \langle \mathbf{r}_{c,j} \cdot \mathbf{r}_{c,j} \rangle. \quad (\text{A3})$$

Here we have assumed that $\mathbf{r}_{c,j}$ do not correlate with each other so that terms $\langle \mathbf{r}_{c,j} \mathbf{r}_{c,i} \rangle$ vanish. Terms $\langle \mathbf{r}_{c,j} \cdot \mathbf{r}_{c,j} \rangle$ corresponding to different arms are statistically equivalent so that the sum over j can be evaluated as

$$\Delta^2 \simeq \frac{1}{f} \langle \mathbf{r}_{c,j} \cdot \mathbf{r}_{c,j} \rangle. \quad (\text{A4})$$

Here we have related Δ to statistical properties of an individual arm, i.e., a linear polymer N monomers long. From scaling arguments we may conclude that $\langle \mathbf{r}_{c,j} \cdot \mathbf{r}_{c,j} \rangle \propto R_{g,j}^2$, where $R_{g,j}$ is the radius of gyration of j th arm. Below we obtain the exact relation between the gyration radius of a star and Δ .

By definition, the radius of gyration of j th arm is related to the position of its center of mass as

$$R_{g,j}^2 = \frac{1}{N} \sum_{i=1}^N \langle (\mathbf{r}_{ij} - \mathbf{r}_{c,j})^2 \rangle \quad (\text{A5})$$

$$= -\langle \mathbf{r}_{c,j} \cdot \mathbf{r}_{c,j} \rangle + \frac{1}{N} \sum_{i=1}^N \langle \mathbf{r}_{ij} \cdot \mathbf{r}_{ij} \rangle. \quad (\text{A6})$$

We note that $\langle \mathbf{r}_{ij} \cdot \mathbf{r}_{ij} \rangle = \sigma^2 i^{2\nu}$ and convert the sum in Eq. (A6) into an integral:

$$\frac{1}{N} \sum_{i=1}^N \langle \mathbf{r}_{ij} \cdot \mathbf{r}_{ij} \rangle = \frac{1}{N} \int_{i=0}^N \sigma^2 i^{6/5} di = \frac{5}{11} \sigma^2 N^{6/5}. \quad (\text{A7})$$

The relation between the mean-squared end-to-end distance, $\sigma^2 N^{6/5}$, and the radius of gyration of a linear polymer can be calculated using $R_{g,j}^2 = \frac{1}{2N^2} \sum_{ik} (r_{ij} - r_{kj})^2$ and replacing the sum by an integral as well. This gives $R_{g,j}^2 = \frac{25}{176} \sigma^2 N^{6/5}$,

which is close to values obtained earlier in MC simulations [32,34],

$$R_{g,j}^2 = (0.157 \pm 0.02) \sigma^2 N^{6/5}. \quad (\text{A8})$$

Now we get $\langle \mathbf{r}_{c,\text{arm}} \cdot \mathbf{r}_{c,\text{arm}} \rangle = \frac{11}{5} R_{g,j}^2$ and substitute this expression into Eq. (A4) to obtain

$$\Delta^2 = \frac{11}{5f} R_{g,j}. \quad (\text{A9})$$

We can now divide this by the radius of gyration of a star $R_g = R_{g,j} (2)^{3/5} (f/2)^{1/5}$, where $R_{g,j}$ is the gyration radius of a single arm, to get

$$\Delta / R_g = \sqrt{\frac{11}{5}} 2^{-2/5} f^{-7/10} \simeq 1.12 f^{-7/10}. \quad (\text{A10})$$

Note that similar analysis using Eq. (A8) leads to

$$\Delta / R_g \simeq 1.044 f^{-7/10}. \quad (\text{A11})$$

APPENDIX B: MC SIMULATIONS

We use explicit (monomer-resolved) model of SPs with f arms. Each arm is made of N Lennard-Jones beads (monomers) subsequently connected by simple harmonic springs:

$$U_{\text{sp}} = \frac{k_{\text{sp}}(r - r_0)^2}{2}. \quad (\text{B1})$$

One end of each arm is connected to the central bead while the other remains free. Nonbonded interactions between monomers are implemented via the Lennard-Jones potential:

$$U_{\text{LJ}}(r) = \begin{cases} 4\epsilon_{\text{LJ}} \left[\left(\frac{\sigma}{r} \right)^{12} - \left(\frac{\sigma}{r} \right)^6 \right], & r < 3\sigma, \\ 0, & r \geq 3\sigma. \end{cases} \quad (\text{B2})$$

We set $k_{\text{sp}} = 2.0k_B T / \sigma^2$, $\epsilon_{\text{LJ}} = 0.05k_B T$, $r_0 = 1.0\sigma$ and vary N from 17 to 49. These parameters correspond to the good solvent regime.

The initial conformations of SP’s arms are generated by performing f random walks that consist of N steps, the length of each step is 1.12σ . Each random walk is started from the central bead and at each step a monomer is placed. The initial conformation is followed by at least $300 \times fN$ equilibration steps. Physical properties of the system are measured after such equilibration and then averaged over at least 50 000 independent conformations. We employ two types of nonlocal moves (each with probability 5%) to accelerate the sampling of the configuration space: we either pivot a randomly chosen arm around a bead or displace a SP as a whole by 1.0σ in random direction. In all other cases we perform single-bead local moves with 0.5σ . We follow Metropolis algorithm with step acceptance probability given by $\min(1, e^{-\Delta U / k_B T})$, where ΔU is the change in the potential energy of the system after a trial move. For the free-energy measurements the total potential energy of the system was modified to include the bias potential $U \rightarrow U - U_B(d)$, which ensures efficient sampling of the configuration space.

The interaction free energy of two SPs is found using the histogram method [22,23]. During the simulation we calculate average radial distribution function (rdf) for the centers of mass for two stars, $g(d)$. The (unbiased) interaction free energy is then given by Boltzmann inversion as

$$F(d) = -k_B T \ln g'(d) + U_b(d), \quad (\text{B3})$$

where $g'(d)$ is the biased rdf and $U_b(d)$ is the bias potential. For calculating F_1 we chose

$$U_b(d) = -\ln 4\pi d^2 + F_0 f^{3/2} \exp\left(-\frac{3d^2}{4R_g^2}\right). \quad (\text{B4})$$

A histogram is sampled in the range $d = 0-35\sigma$ with a resolution of $0.2-0.35\sigma$ per bin. To obtain F_2 we perform the same simulations as described above, but connect two SPs via two of their outermost beads. The bias potential in this case was chosen to be

$$U_B(d) = -\ln 4\pi d^2 + F_0 f^{3/2} \exp\left(-\frac{3d^2}{4R_g^2}\right) + \frac{1}{2}kd^2. \quad (\text{B5})$$

We verify the model for the bridge potential, Eq. (8), by calculating the effective potential F_2 between centers of mass of two bridged stars of $f = 4$ and N varying from 17 to 49. We then obtain values of k by employing Eq. (7) and taking k as the only adjustable parameter. The results are shown in Fig. 8. We also calculated the effective potential between the ends of a linear chain of $2N$ monomers, which corresponds to F^b alone. The deduced values of stiffness of linear chains agree well with the stiffness of a bridge between two stars and confirm the model described by Eq. (8).

APPENDIX C: PROBABILITY OF COLLISION OF HARD-SPHERE BROWNIAN PARTICLES

A short-range contribution to the free energy of interaction between two SPs is given by $F^{\text{hs}} = -k_B T \ln Z(d)/Z(\infty)$, where $Z(d)$ is the number of allowed configurations of two dense cores in a situation when centers of mass of SPs are separated by d . To estimate $Z(d)$, we exclude from $Z(\infty)$ all the forbidden configurations, i.e., those that lead to an overlap of two cores, $Z(d) = Z(\infty) - Z_{\text{overlap}}(d)$. Thus, the free energy can be written as $F^{\text{hs}} = -k_B T \ln(1 - P)$, where $P = Z_{\text{overlap}}/Z(\infty)$ is the probability that two cores overlap, i.e., the distance between them is less than $2\sigma_c$. We can now find P as a function of d and Δ .

Due to the statistical properties of SPs' dense cores described in Appendix A, we treat them as Brownian particles where Δ^2 defines a characteristic time scale, hence we may reduce the task of finding P to a single-particle diffusion problem. To achieve that, we note that the probability of two Brownian particles of radius σ_c overlapping after the time t is equal to that of a pointlike Brownian particle overlapping with a stationary one of radius $2\sigma_c$ after a time $2t$. To calculate P , we locate the stationary particle at a point $\{0,0,d\}$ and the pointlike Brownian particle at $\{0,0,0\}$. The probability density of a pointlike Brownian particle being at $\{x,y,z\}$ after a time

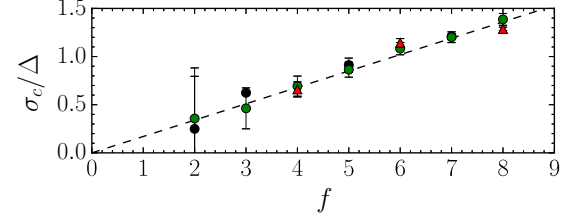


FIG. 12. The ratio of the effective core size to Δ as a function of f obtained in simulations (symbols) by using $N = 17$ (circles), 25 (squares), and 49 (triangles). Dashed line shows $\sigma_c/\Delta = 0.16f$.

interval of $2t$ is given by [35]

$$p(x,y,z,2t) = \frac{\exp\left(-\frac{x^2+y^2+z^2}{8Dt}\right)}{(8\pi Dt)^{3/2}}. \quad (\text{C1})$$

The probability of overlap, $P(t,d)$, is the probability that the pointlike Brownian particle will be at $\sqrt{x^2 + y^2 + (z-d)^2} \leq 2\sigma_c$ at time $2t$:

$$P(t,d) = \iiint_{\sqrt{x^2+y^2+(z-d)^2} \leq 2\sigma_c} dx dy dz p(x,y,z,2t). \quad (\text{C2})$$

After shifting the variable $z \rightarrow z + d$ and rewriting this expression in spherical coordinates it becomes

$$P(t,d) = \int_0^R dr \int_0^\pi d\theta \frac{2\pi r^2 \sin\theta}{(8\pi Dt)^{3/2}} e^{-\frac{r^2+2rd\cos\theta+d^2}{8Dt}}. \quad (\text{C3})$$

We can evaluate the integral and substitute $6Dt$ for Δ^2 to obtain

$$P = \frac{1}{2}\text{erf}(y_-) - \frac{1}{2}\text{erf}(y_+) + \sqrt{\frac{\Delta^2}{3\pi d^2}}(e^{-y_-^2} - e^{-y_+^2}), \quad (\text{C4})$$

where $y_\pm = \frac{\sqrt{3}}{2} \frac{d \pm 2\sigma_c}{\Delta}$. Note that this task is different from a commonly considered case of diffusion limited aggregation [36,37] or first passage problems [38,39] because we evaluate whether the particles overlap *after* a certain time $2t$, while any collisions before $2t$ are allowed to take place.

To prove the dependence of the effective core size σ_c on f and N , we fit the free energies of interaction of two SPs, $F(d)$, using Eq. (6) with two adjustable parameters F_0 and σ_c . In Fig. 12 we plot the ratio σ_c/Δ as a function of f for $N = 17, 25, 49$ and $f = 2-8$. We find that the simulation data agrees well with the scaling $\sigma_c/\Delta = Bf$, where we find $B = 0.16 \pm 0.02$. This single value of B is chosen for all calculations of the free energies of interaction and is not further used as an adjustable parameter.

APPENDIX D: EXPLICIT AND COARSE-GRAINED MD SIMULATIONS OF POLYMER NETWORKS

We measure the pressure in a polymer network upon its deformation in coarse-grained and explicit MD computer simulations. In the case of an infinite explicit network we simulate 2^3 SPs of $f = 6$ connected by bridges of $2N = 34$. SPs are connected in a cubic lattice with the corresponding periodic images. The volume of the network is varied by equally changing each side of the simulation cell: $L \rightarrow \lambda L$. Particles' coordinates are also rescaled in accordance with $x_i \rightarrow \lambda x_i, y_i \rightarrow \lambda y_i, z_i \rightarrow \lambda z_i$.

Initially, the network is set up in a stretched state with the box size $L/d_0 = 3.0$, which is then sequentially reduced to $L/d_0 = 0.75$ in 100 volume reduction steps. After each volume reduction step the system is equilibrated for at least 3×10^4 MD steps. The MD time step is set as $\Delta t = 0.001 \sqrt{m\sigma^2/k_B T}$, where m is the monomer mass.

The random networks are prepared using the following sequence: we randomly place 64 junction beads in a box of size $L/d_0 = 3.0$ and randomly designate a functionality f_i , varied from 3 to 7, to i th bead. After that, for each bead we choose f_i closest neighbors (including virtual images) and connect them via bridges of $2N = 34$ monomers. Due to inherent randomness this algorithm can produce networks that are too loose, with periodicity preserved only by a few subchains, hence some selection technique is in order. For the sake of simplicity we view each generated network as a non-periodic graph and select only those configurations, that are k -connected with $k = 3$, and have minimal radius, to ensure that our networks are as branched as possible. Using these criteria, we select approximately 300 configurations out of the initial 4000, and consequently choose three networks at random for the simulation of anisotropic compression and extension. These networks are initially equilibrated and then brought to a stress-free state by rescaling the size of the simulation box. Then the box is stretched along z axis to the value of $L_z/d_0 = 2.5$ at a constant volume (meaning that L_x and L_y are rescaled accordingly) and gradually compressed along z up to $L_z/d_0 = 0.2$, again, keeping the volume the same.

The pressure tensor is calculated using the virial theorem where we take into account pairwise interactions between monomers:

$$\Pi_{kl} = \left\langle \frac{\sum_i m_i v_i^{(k)} v_i^{(l)}}{V} + \frac{1}{V} \sum_{i < j} f_{ij}^{(k)} r_{ij}^{(l)} \right\rangle_t. \quad (\text{D1})$$

Here V is volume of the simulation box, $f_{ij}^{(k)}$ is the k th component of the force on particle i exerted by particle

j . It is calculated using the interatomic potentials given by Eqs. (B1)–(B2):

$$\mathbf{f}_{ij} = \frac{\mathbf{r}_{ij}}{r_{ij}} \frac{\partial}{\partial r_{ij}} [U_{LJ}(r_{ij}) + U_{sp}(r_{ij})], \quad (\text{D2})$$

where $\mathbf{r}_{ij} = \mathbf{r}_j - \mathbf{r}_i$ is a vector starting at the position of particle i , r_{ij} is the distance between particles i and j , m_i and \mathbf{v}_i are the mass and velocity of particle i correspondingly. $\langle \dots \rangle_t$ denotes time average over at least 100 independent configurations. Isotropic excess pressure is then given by $(\Pi_{xx} + \Pi_{yy} + \Pi_{zz})/3$.

We perform the simulation of a coarse-grained network by replacing each star with a coarse-grained particle that interacts with its bridged neighbours with via potential F_2 and with the rest of the particles via potential F_1 . The cutoff radius for the latter interaction was chosen as $r_{\text{cut}} = 40\sigma$. The MD time step is set as $\Delta t = 0.001 \sqrt{M\sigma^2/k_B T}$, where $M = fNm$ is the SP's mass. The pressure tensor of a coarse-grained system is calculated using the virial theorem theorem where pairwise interactions between coarse-grained particles are taken into account:

$$\Pi_{kl} = \frac{N_{\text{SP}} k_B T}{V} + \left\langle \frac{1}{3V} \sum_{i < j} \mathbf{f}_{ij}^{(k)} \mathbf{r}_{ij}^{(l)} \right\rangle_t. \quad (\text{D3})$$

Here N_{SP} is the number of stars in the simulation box. The forces \mathbf{f}_{ij} between coarse-grained particles are calculated using potentials $F_{1,2}$:

$$\mathbf{f}_{ij} = \frac{\mathbf{r}_{ij}}{r_{ij}} \frac{\partial}{\partial r_{ij}} [F_1(r_{ij}) + F_2(r_{ij})].$$

The number of coarse-grained particles in the unit cell is varied in the range $2^3 - 20^3$. Pressure is found to be independent on the number of cubic unit cells.

-
- [1] G. C. Claudio, K. Kremer, and C. Holm, *J. Chem. Phys.* **131**, 094903 (2009).
- [2] A. M. Romyantsev, A. A. Rudov, and I. I. Potemkin, *J. Chem. Phys.* **142**, 171105 (2015).
- [3] B. A. Mann, C. Holm, and K. Kremer, *J. Chem. Phys.* **122**, 154903 (2005).
- [4] B. A. F. Mann, K. Kremer, O. Lenz, and C. Holm, *Macromol. Theor. Simul.* **20**, 721 (2011).
- [5] A. A. Gavrilov and A. V. Chertovich, *Polym. Sci. Ser. A* **56**, 90 (2014).
- [6] J. Zidek, J. Jancar, A. Milchev, and T. A. Vilgis, *Macromolecules* **47**, 8795 (2014).
- [7] H. Masoud and A. Alexeev, *ACS Nano* **6**, 212 (2012).
- [8] T. A. Witten and P. A. Pincus, *Macromolecules* **19**, 2509 (1986).
- [9] C. N. Likos, H. Löwen, M. Watzlawek, B. Abbas, O. Jucknischke, J. Allgaier, and D. Richter, *Phys. Rev. Lett.* **80**, 4450 (1998).
- [10] A. Jusufi, J. Dzubiella, C. N. Likos, C. Von Ferber, and H. Löwen, *J. Phys.: Condens. Matter* **13**, 6177 (2001).
- [11] D. K. Rai, G. Beaucage, K. Ratkanthwar, P. Beaucage, R. Ramachandran, and N. Hadjichristidis, *Phys. Rev. E* **93**, 052501 (2016).
- [12] G. Chen, H. Li, and S. Das, *J. Phys. Chem. B* **120**, 5272 (2016).
- [13] A. M. Rubio and J. J. Freire, *Comput. Theor. Polym. S.* **10**, 89 (2000).
- [14] A. A. Louis, P. G. Bolhuis, J. P. Hansen, and E. J. Meijer, *Phys. Rev. Lett.* **85**, 2522 (2000).
- [15] A. A. Louis, P. G. Bolhuis, and J. P. Hansen, *Phys. Rev. E* **62**, 7961 (2000).
- [16] P. G. Bolhuis, A. A. Louis, J. P. Hansen, and E. J. Meijer, *J. Chem. Phys.* **114**, 4296 (2001).
- [17] B. Kruger, L. Schäfer, and A. Baumgärtner, *J. Phys. (Paris)* **50**, 3191 (1989).
- [18] A. M. Rubio and J. J. Freire, *Macromolecules* **29**, 6946 (1996).
- [19] T. Sakai, T. Matsunaga, Y. Yamamoto, C. Ito, R. Yoshida, S. Suzuki, N. Sasaki, M. Shibayama, and U.-I. Chung, *Macromolecules* **41**, 5379 (2008).

- [20] T. Matsunaga, T. Sakai, Y. Akagi, U.-I. Chung, and M. Shibayama, *Macromolecules* **42**, 1344 (2009).
- [21] M. Daoud and J. P. Cotton, *J. Phys. France* **43**, 531 (1982).
- [22] D. Frenkel and B. Smit, *Understanding Molecular Simulation*, 2nd ed. (Academic Press, Orlando, FL, 2001).
- [23] A. M. Ferrenberg and R. H. Swendsen, *Phys. Rev. Lett.* **63**, 1195 (1989).
- [24] C. N. Likos, M. Schmidt, H. Löwen, M. Ballauff, D. Pötschke, and P. Lindner, *Macromolecules* **34**, 2914 (2001).
- [25] P. J. Flory and W. R. Krigbaum, *J. Chem. Phys.* **18**, 1086 (1950).
- [26] M. Daoud, J. P. Cotton, B. Farnoux, G. Jannink, G. Sarma, H. Benoit, C. Duplessix, C. Picot, and P. G. de Gennes, *Macromolecules* **8**, 804 (1975).
- [27] A. Y. Grosberg, P. G. Khalatur, and A. R. Khokhlov, *Macromol. Rapid Commun.* **3**, 709 (1982).
- [28] P.-G. de Gennes, *Scaling Concepts in Polymer Physics* (Cornell University Press, Ithaca, NY, 1979).
- [29] P. J. Flory, *Principles of Polymer Chemistry* (Cornell University Press, Ithaca, NY, 1953).
- [30] P. Pincus, *Macromolecules* **9**, 386 (1976).
- [31] A. Y. Grosberg and A. R. Khokhlov, *Statistical Mechanics of Macromolecules* (American Institute of Physics, College Park, MD, 1994).
- [32] F. T. Wall and J. J. Erpenbeck, *J. Chem. Phys.* **30**, 637 (1959).
- [33] H.-J. Limbach, A. Arnold, B. A. Mann, and C. Holm, *Comput. Phys. Commun.* **174**, 704 (2006).
- [34] F. L. McCrackin, J. Mazur, and C. M. Guttman, *Macromolecules* **6**, 859 (1973).
- [35] S. Redner, *A Guide to First-Passage Processes* (Cambridge University Press, Cambridge, 2001).
- [36] A. Szabo, K. Schulten, and Z. Schulten, *J. Chem. Phys.* **72**, 4350 (1980).
- [37] B. J. Ackerson, *J. Chem. Phys.* **64**, 242 (1976).
- [38] D. A. Darling and A. J. F. Siegert, *Ann. Math. Stat.* **24**, 624 (1953).
- [39] U. Sumita and Y. Masuda, *Stoch. Proc. Appl.* **20**, 133 (1985).